

Porous Organic Crystals

Highly Stable Single Crystals of Three-Dimensional Porous Oligomer Frameworks Synthesized under Kinetic Conditions

Linxiao Hou⁺, Chuan Shan⁺, Yanpei Song, Sifan Chen, Lukasz Wojtas, Shengqian Ma,^{*} Qi Sun,^{*} and Lin Zhang

Abstract: Various robust, crystalline, and porous organic frameworks based on *in situ*-formed imine-linked oligomers were investigated. These oligomers self-assembled through collaborative intermolecular hydrogen bonding interactions via liquid–liquid interfacial reactions. The soluble oligomers were kinetic products with multiple unreacted aldehyde groups that acted as hydrogen bond donors and acceptors and directed the assembly of the resulting oligomers into 3D frameworks. The sequential formation of robust covalent linkages and highly reversible hydrogen bonds enforced long-range symmetry and facilitated the production of large single crystals, with structures that were unambiguously determined by single-crystal X-ray diffraction. The unique hierarchical arrangements increased the steric hindrance of the imine bond, which prevented attacks from water molecules, greatly improving the stability. The multiple binding sites in the frameworks enabled rapid sequestration of micropollutant in water.

Introduction

Porous materials are essential in applications, such as separation and catalysis,^[1] and can potentially be applied in other contexts, such as sorbents for water purification.^[2] Sustained efforts have been devoted to the manipulation of spatial arrangement of molecular units for enabling the design of advanced functional and porous materials. The tremendous progress in modular construction, wherein molecular building blocks are predicted to form neighboring struts, has led to extensive research on porous materials based on various concepts, such as supramolecular frameworks assembled via noncovalent interactions,^[3] metal–organic frameworks

(MOFs) linked by coordination bonds,^[4] and covalent organic frameworks (COFs) held together by covalent bonds.^[5] In contrast to supramolecular networks and MOFs, attempts to create monocrystalline porous frameworks with covalent linkages have been thwarted; the continuous formation and breakage of strong covalent bonds to enforce long-range symmetry has proven to be exceedingly difficult.^[6] The lack of atomically precise structural details has considerably impaired the determination of structure–property correlations that drive the material discovery process and are essential for improving the properties of existing porous materials. Porous 3D COF single crystals suitable for single-crystal X-ray diffraction (SCXRD) analysis were successfully obtained recently using aniline modulators that enhanced the reversibility of imine bond formation and consequentially improved the crystallization.^[7] Numerous fundamental questions pertaining to the degree of interpenetration and guest arrangement in the reported COFs were answered. Strategies to limit the formation of covalent bonds during crystallization can further facilitate the development of porous single-crystal materials.

The production of polycrystalline powders can be inherently predisposed to uncontrolled growth processes compared to that of single crystals; therefore, the introduction of noncovalent interactions was postulated in the present study to enhance the error correction process in crystallization with respect to the formation of covalent bonds.^[8] However, because the noncovalent interactions are much more reversible than covalent bonds, they usually dominate crystal growth, which, in turn, abstracts the covalent linkage formation, similar to that observed in 2D COFs. Moreover, the noncovalent bonds are too weak to enforce long-range symmetry, leading to severe stacking disorder.

Therefore, a balance between reversibility and robustness of the connecting bonds was hypothesized, provided that the noncovalent linkages occurred after the formation of covalent bonds, which could ultimately result in enhanced crystal growth. Controlling the formation of polymerization intermediates was theorized to efficiently alter the crystallization process. Unlike materials synthesized under solvothermal conditions, which typically result in thermodynamic products isolated as powders comprising aggregated nanometer-scale crystallites, liquid–liquid interfacial reactions performed under ambient conditions can generate soluble and kinetic stable intermediates; this can facilitate a greater control over the crystallization process.



In this study, a general approach involving liquid–liquid interfacial crystallization was investigated to facilitate the

[*] Dr. L. Hou,^[†] S. Chen, Dr. Q. Sun, Prof. L. Zhang
Zhejiang Provincial Key Laboratory of Advanced Chemical Engineering Manufacture Technology, College of Chemical and Biological Engineering, Zhejiang University
Hangzhou, 310027 (China)
E-mail: sunqichs@zju.edu.cn

C. Shan,^[†] Dr. L. Wojtas
Department of Chemistry, University of South Florida
4202 E. Fowler Avenue, Tampa, FL 33620 (USA)

Y. Song, Prof. S. Ma
Department of Chemistry, University of North Texas
1508 W Mulberry St, Denton, TX 76201 (USA)
E-mail: shengqian.ma@unt.edu

[†] These authors contributed equally to this work.

 Supporting information and the ORCID identification number(s) for the author(s) of this article can be found under:
 <https://doi.org/10.1002/anie.202103729>.

growth of large and porous organic single crystals. These were self-assembled via intermolecular hydrogen bonding, based on in situ-formed oligomers linked by imine bonds that were formed via condensation between tetra-topic amine and di-topic aldehyde compounds; this eventually led to the formation of hydrogen-bonded organic frameworks (HOFs). This hierarchical assembly was found to produce monocrystalline framework structures that were amenable for SCXRD analysis; these synthesized structures are the first representative examples of as-synthesized porous oligomer single crystals. The structural stability of the resulting HOFs was confirmed through their exceptional tolerance against a wide range of solvents and pH environments; the framework structure remained sufficiently robust even after solvent removal and offered accessible porosity that was comparable, or even superior, to that of COF analogues; these results revealed their extraordinary potential for application in various fields.

Results and Discussion

As a proof of concept, tetrakis(4-aminophenyl)methane (TAM) was reacted with dialdehyde compounds under liquid–liquid interface. TAM was dissolved in a 3 M aqueous acetic acid solution, followed by gentle layering of a dialdehyde mixture of mesitylene/ethyl acetate (V/V = 1/3) on top of the aqueous solution by ensuring that the solution was undisturbed. Unlike materials prepared under solvothermal conditions, which often produce polycrystalline or amorphous products, materials synthesized via interfacial polymerization yield visible needle-shaped crystals in the organic phase. A comprehensive screening of synthetic conditions revealed that the use of ethyl acetate and mesitylene in their respective ratios was intended to control the solubility of the starting materials and to maximize the crystallinity of the products. The formation of large crystals was observed after the appearance of a yellowish film at the liquid–liquid boundary, which revealed the predominance of nucleation when the two phases were mixed. However, after the interface was blocked, the diffusion of the amine compound into the organic phases significantly decreased, leading to the suspension of nucleation, which is conducive to crystallite growth. Therefore, to obtain high-quality single crystals in the structure solution, a polyacrylonitrile (PAN) ultrafiltration membrane was placed at the interface to control the diffusion of amine compounds into the organic phase (Supporting Information, Figure S1). Optical microscopy and scanning electron microscopy (SEM) analyses revealed that morphologically uniform crystallites with lengths ranging from 60 to 100 μm were isolated (Supporting Information, Figures S2 and S3).

SCXRD studies revealed that HOF-TAM-BDA, which was synthesized using TAM and 4,4'-biphenyldicarbaldehyde (BDA), crystallized in the high-symmetry tetragonal space group $I41/a$ with unit-cell parameters of $a = b = 30.7006 \text{ \AA}$, $c = 7.6610 \text{ \AA}$, and a unit-cell volume of 7220.7 \AA^3 (Table S1 and Figure S4). Structural analysis of HOF-TAM-BDA indicated that there was one-fourth of the tetra-imine oligomer in the asymmetric unit, which resulted from the

preliminary imine condensation between TAM and four equivalents of BDA after eliminating four equivalents of water (Figure 1a). Further examination of the symmetrically expanded structure revealed two important features. First, a translation of 7.65 \AA along the main axis correlated two mutually interlacing tetra-imine oligomers with C–H \cdots N interactions, which further bonded as a “tenoned” oligomer strand in the crystallographic c direction. This arrangement was noted to be similar to that of the TAM moiety in the COF-320 structure, which was synthesized from the condensation of TAM and BDA under solvothermal conditions,^[9] whereas the second feature places them into distinct hierarchies. In the structure produced in this study, each unreacted aldehyde group served as hydrogen bond donors for the lone pair of carbonyl oxygen on the adjacent oligomer in the same strand ($d(\text{C–H}\cdots\text{O}) = 2.612 \text{ \AA}$), as well as the lone pair of imine nitrogen on the side branch of the antiparallel oligomer that extended from another strand ($d(\text{C–H}\cdots\text{N}) = 3.063 \text{ \AA}$). Hydrogen bonding enhanced the stability of a single oligomer strand, whereas the C–H \cdots N hydrogen bonding, which was absent in the COF-320 structure, essentially behaved as a “Velcro strip” that buckled the oligomer strands into an arrangement with highly robust structural integrity (Figure 1b). Additionally, a strong hydrogen bonding interaction was noted to be present between the aromatic hydrogen and the neighboring nitrogen in the imine group (C–H \cdots N) at a distance of 3.057 \AA (Figure 1b). The unique packing resulted in an assembly that featured one-dimensional and quasi-square-shaped pores parallel to the crystallographic c axis with a pore diameter of 10.6 \AA , in which a certain amount of disordered solvent molecules resided (Figure 1c). Mesitylene molecules were identified in the electron density map and refined using restraints. Analysis via the PLATON software revealed that the solvent-accessible free volume of the channels and molecular cavities in HOF-TAM-BDA was 24.8% of the total crystal volume and the solvent accessible surface area calculated from the guest-free single crystal structure was $899 \text{ m}^2 \text{ g}^{-1}$.

To confirm the role of the unreacted aldehyde group during self-assembly, comparative studies of the packing diagrams of single crystals synthesized via the condensation of TAM and 4-phenylbenzaldehyde were conducted (Supporting Information, Figure S5, OF-TAM-PBA). The results revealed that the interactions between oligomer molecules were significantly weaker; neither strong hydrogen bonding interactions nor π - π stacking was observed. Therefore, these results supported the hypothesis that chemical transformation and the direction of hydrogen bonding synergistically contributed to program the assembly of HOFs.

Matrix-assisted laser desorption/ionization time-of-flight mass spectrometry (MALDI-TOF MS) studies provided mechanistic insights, as well as direct evidence of the formation of oligomer frameworks. The peak at m/z 1149.6 was observed to be the primary signal of the crystalline material, which coincided with that of the expected oligomer (m/z 1149.3); a similar peak was also observed for the film formed at the interface (Supporting Information, Figure S6). This similarity in composition was further confirmed using Fourier-transform infrared (FTIR) spectroscopy (Supporting

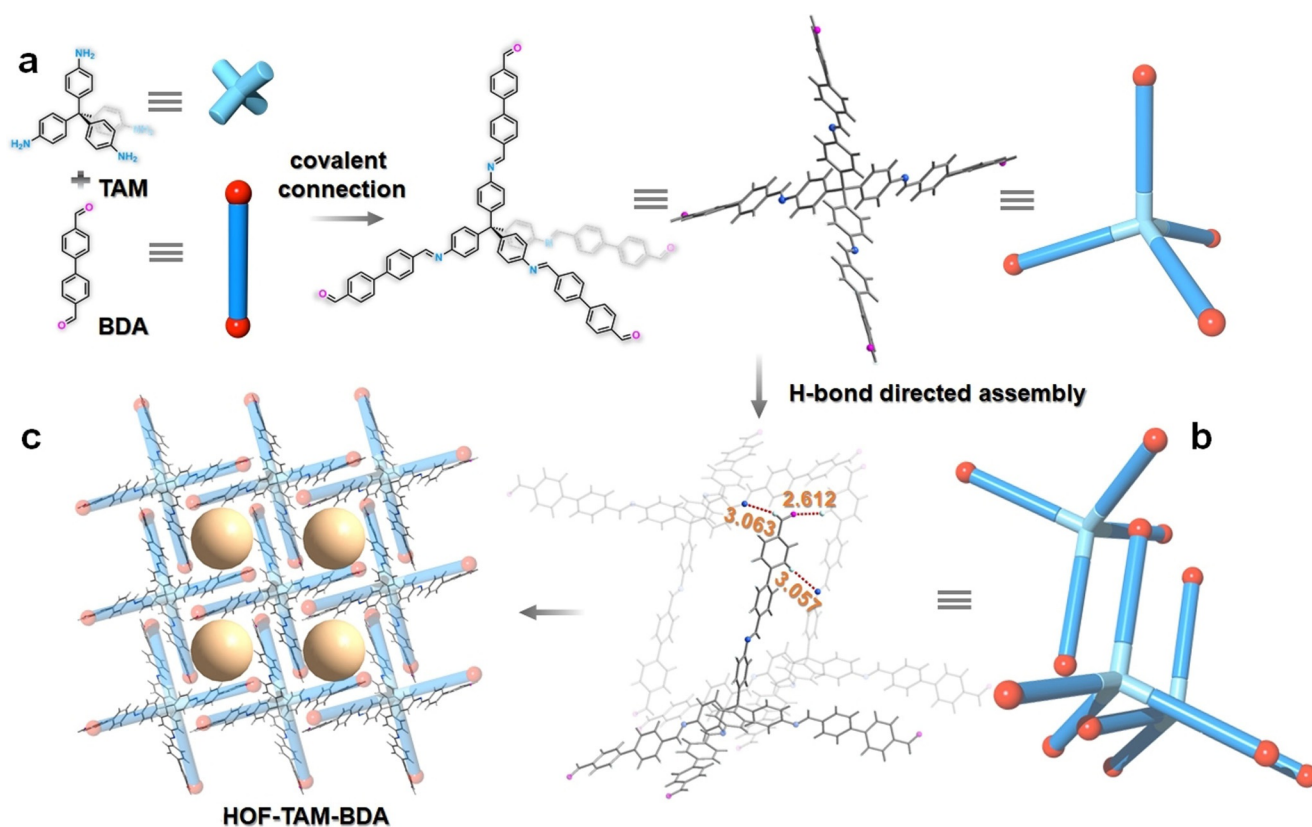


Figure 1. Single-crystal structure of HOF-TAM-BDA.^[12] a) Synthesis of the oligomer constructed for HOF-TAM-BDA. b), c) X-ray crystal structure of HOF-TAM-BDA featuring multiple hydrogen bonding (red dashed lines) among adjacent units to form 3D framework exhibiting quasi square-shaped pores with a diameter of about 10.6 Å along the *c* axis. The unit of hydrogen bond length is Å. For clarity, only hydrogen atoms that have hydrogen bonding interactions with the guest molecule are shown (C gray, N blue, O magenta, H light cyan).

Information, Figure S7), which suggested that the TAM molecules that permeated into the organic phase were quickly consumed owing to a large excess of aldehyde; the self-assembly of the generated oligomers into a framework, instead of reacting further to eventually form COF, was also confirmed. Therefore, these results suggest that the compositions of certain previously reported 3D COFs be re-examined, because powder X-ray diffraction (PXRD) or even solid-state nuclear magnetic resonance (NMR) may not be sufficient for structural validation in such cases, especially under interface polymerization conditions, that is, kinetic conditions.

PXRD analysis of the isolated crystals indicated the uniformity of HOF and did not reveal any diffraction peak that could be attributed to the monomers. To confirm that the single-crystal structure was representative of the bulk sample, the experimental powder pattern was compared to that calculated using the single-crystal structures. A close correspondence was noted between the peak positions, which substantiated the phase purity (Figure 2a; Supporting Information, Figure S8). Unsurprisingly, the relative peak intensity differed greatly because of the preferred orientation commonly found in crystals with an acicular crystal habit; this could be explained using the PXRD pattern of the HOF-TAM-BDA powder formed at the interface. Thermogravimetric analysis (TGA) suggested that the guest molecules in HOF-TAM-BDA could be removed to yield desolvated

material that was stable up to 300 °C (Supporting Information, Figure S9).

To explore the chemical stability of HOF-TAM-BDA, its tolerance against various solvents and pH environments was evaluated. After treatment with a broad spectrum of organic solvents, such as CHCl_3 , dimethyl sulfoxide (DMSO), ethanol, and acidic/basic aqueous solutions (pH 0–14), the PXRD results indicated that HOF-TAM-BDA not only maintained its crystalline morphology but also preserved its crystallinity. It is important to note that HOF-TAM-BDA survived strongly acidic conditions, under which the corresponding COF material (COF-320) completely decomposed (Supporting Information, Figures S10–S12). The exceptional chemical stability against hydrolysis, which was significantly greater than that of other imine-linked analogs, was noteworthy. The mechanism of imine hydrolysis comprises the following steps: protonation of imine nitrogen, nucleophilic attack of water to iminium carbon, proton transfer, and elimination of amine. Among these, the elimination step is believed to be the rate-determining step under acidic conditions.^[10] Nevertheless, any factor that can impede the steps prior to the rate-determining step can significantly affect the hydrolysis rate; this corresponds to the nucleophilic attack of water in the present context. The Bürgi-Dunitz angle during the nucleophilic attack on carbonyl compounds can be invoked to elucidate this observation, wherein water molecules were noted to barely perform efficient nucleophilic attacks because the

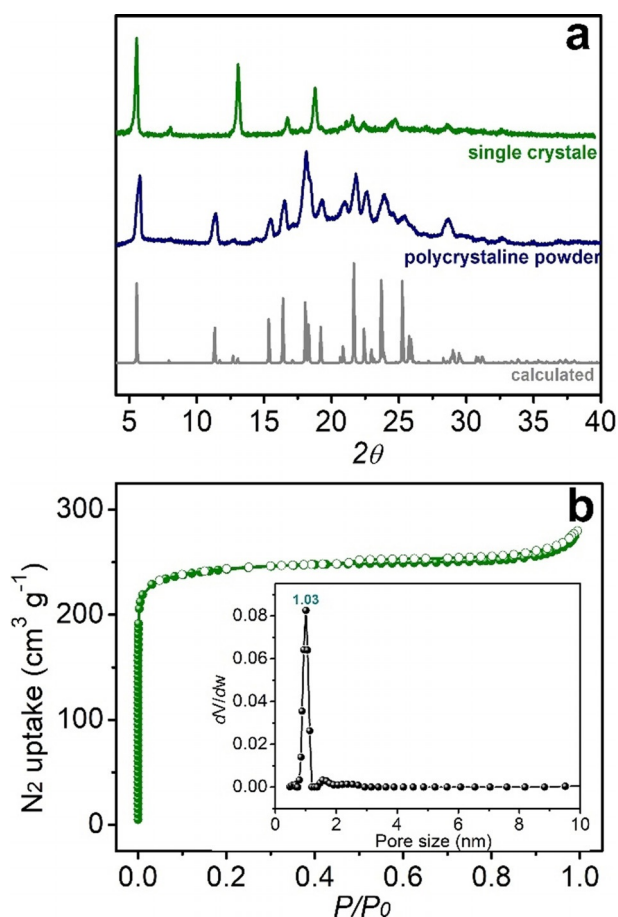


Figure 2. Crystallinity and porosity of the HOF-TAM-BDA. a) Powder X-ray diffraction patterns for the single crystals of HOF-TAM-BDA and the polycrystalline powder formed at the interface (HOF-TAM-BDA powder) compared with the calculated pattern derived from its single-crystal structure. b) N_2 sorption isotherms for HOF-TAM-BDA measured at 77 K and the corresponding pore size distribution derived from the DFT model (inset).

appropriate incoming geometry was inaccessible. In the attached Figure derived using the crystal structure (Figure 3), both sides of the imine plane are observed to be completely blocked from the H_2O molecules arriving from the quasi-square-shaped pores by a hydrogen-bonded aldehyde group or phenyl group on adjacent oligomers. This antiparallel stacking of adjacent oligomer branches from different strands proves to be a key feature that favors hydrolytic stability by blocking water that can attack the imine bond under strongly acidic conditions. Such a characteristic self-protecting and hydrogen-bonded double layer is absent in other COF materials, because oligomer branches link to adjacent branches to form 3D COF branches that are staggered to one another. Notably, the imine linkages were exposed to the pore channel of the model material, COF-320, which completely decomposed in a 1 M HCl aqueous solution within 1 h. The comparison of these structures leads to a conclusion that hydrogen bonding plays a significant role in the improved arrangement and stability of in situ-formed covalent oligomers. This enhancement has also been observed in other materials, such as 2D imine-linked COFs.^[11]

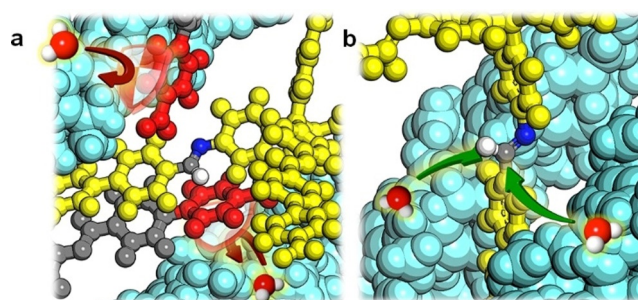


Figure 3. Illustration of the location of imine linkage in a) HOF-TAM-BDA and b) COF-320. Derived from the crystal structures, it can be seen that the imine linkage is crowded by a phenyl ring and aldehyde group in HOF-TAM-BDA, blocking the access of H_2O molecules, while it is exposed to the pore channel in COF-320. The direction of the pore content is highlighted in light cyan, and red atoms indicate unfavorable mass transfer and unfavorable nucleophilic attack of water.

The enhanced stability and open channels in HOF-TAM-BDA prompted an evaluation of its permanent porosity. Activation of HOF-TAM-BDA was accomplished as follows: prior to degassing at 100 °C, the samples were pre-activated by solvent exchanging with hexane and drying under N_2 flow at room temperature to prevent pore collapse. PXRD results indicated no structural changes upon the removal of the guest molecules. N_2 sorption isotherms for HOF-TAM-BDA were collected at 77 K and exhibited a classic type I adsorption behavior characterized by a sharp gas uptake in the low relative-pressure region with $P/P_0 < 0.1$ (Figure 2b). The surface area calculated using the Brunauer–Emmett–Teller (BET) model was $850 \text{ m}^2 \text{ g}^{-1}$ with a pore volume of $0.43 \text{ cm}^3 \text{ g}^{-1}$. The calculation of pore size by fitting the density functional theory model to the adsorption isotherm yielded a narrow distribution centered at 1.03 nm, which was consistent with the pore diameter derived from the crystal structures. However, attempts to activate OF-TAM-PBA with apparent N_2 uptake capacities were unsuccessful, suggesting that the synergistic effect of multiple strong-hydrogen-bonding interactions in HOF-TAM-BDA guaranteed the establishment of permanent porosity and afforded its robustness; this was noted to be similar to that in DNA, where hydrogen bonding plays a fundamental role in the maintenance of secondary and tertiary structures.

The generality of the interface polymerization approach was subsequently demonstrated in two other 3D HOFs, HOF-TAM-BPY and HOF-TAM-PNA, which were assembled via the condensation of TAM with 2,2'-bipyridyl-5,5'-dialdehyde (BPY) and 6-(4-formylphenyl)nicotinaldehyde (PNA), respectively; the growth behaviors of these compounds were similar to that of HOF-TAM-BDA. Both frameworks were crystallized in the same space group of $I4_1/a$, which was considered to be isoreticular to that of HOF-TAM-BDA. BET surface areas of 1307 and $2008 \text{ m}^2 \text{ g}^{-1}$ were obtained in these two HOFs, respectively (Figure 4). The additional C–H...N hydrogen bond between the N atoms in the pyridine moieties and C–H in the adjacent phenyl ring were presumed to further enforce the structure, which resulted in higher surface areas than that of HOF-TAM-BDA (Supporting Information, Figures S13–S26, Tables S2 and S3).

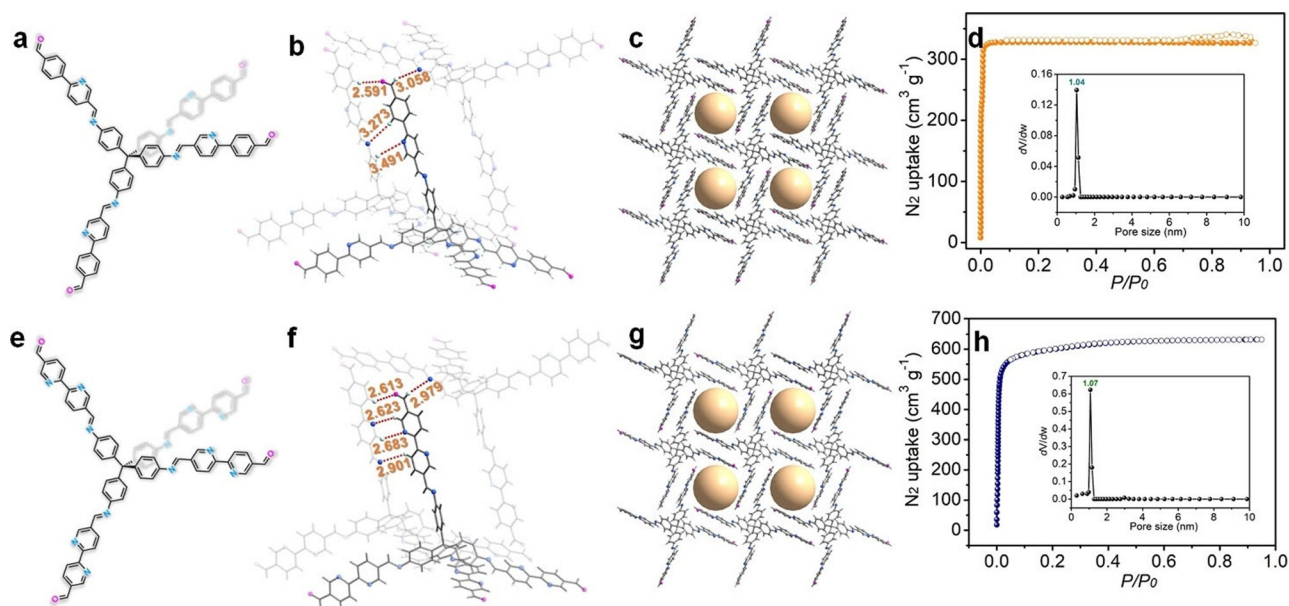


Figure 4. Crystal structure and porosity of HOF-TAM-PNA and HOF-TAM-BPY.^[12] a),e) The chemical structures of the oligomers constructed for HOF-TAM-PNA and HOF-TAM-BPY. b),c) X-ray crystal structure of HOF-TAM-PNA and f),g) HOF-TAM-BPY featuring multiple hydrogen bonding (red dashed lines) among adjacent units to form 3D framework exhibiting quasi square-shaped pores along the *c* axis. For clarity, only hydrogen atoms that have hydrogen bonding interactions with the guest molecule are shown (C gray, N blue, O magenta, H light cyan). The unit of hydrogen bond length is Å. d),h) N₂ sorption isotherms for HOF-TAM-PNA and HOF-TAM-BPY, respectively, measured at 77 K and the corresponding pore-size-distribution derived from the DFT model (inset).

The structural features revealed thus far prompted an investigation of their applications for addressing the challenging issue of water purification. Research in the medical industry and animal husbandry have led to great improvements over the last century in several aspects; however, these advances have also led to severe adverse effects relating to the release of pharmaceuticals into the environment.^[2] Ofloxacin, a widely used antibiotic that has caused great concern as an immune disruptor, was selected as a model organic micropollutant. To demonstrate the superiority of the synthesized HOFs as sorbent materials, the ofloxacin sorption performance of HOF-TAM-BDA was benchmarked with COF-320, active carbon (Aladdin, BET: 1113 m² g⁻¹), and MCM-41 (Sigma-Aldrich, BET: 1008 m² g⁻¹; Supporting Information, Figures S27–S31). HOF-TAM-BDA (1 mg mL⁻¹) eventually removed more than 99% of ofloxacin from an aqueous solution of 20 ppm, whereas COF-320, active carbon, and MCM-41 removed only 67%, 41%, and 16% of the ofloxacin, respectively, under otherwise identical conditions. Moreover, HOF-TAM-BDA captured ofloxacin at a significantly faster rate than those of other adsorbents, and achieved 96% of its equilibrium uptake only within 2 min. By contrast, COF-320 required 120 min to reach equilibrium and captured only 16.1% of its equilibrium value after 2 min (Figure 5 a). Active carbon and MCM-41 required more than 180 min to reach equilibrium. The near-instantaneous ofloxacin trapping of HOF-TAM-BDA could be attributed to its unique adsorption sites, which have superior ofloxacin affinity than those of other adsorbents. Specifically, the initial ofloxacin adsorption rate for HOF-TAM-BDA was 140.92 mg g⁻¹ min⁻¹, which was more than two or three orders of magnitude greater than those of COF-320 (0.95 mg g⁻¹ min⁻¹), active carbon

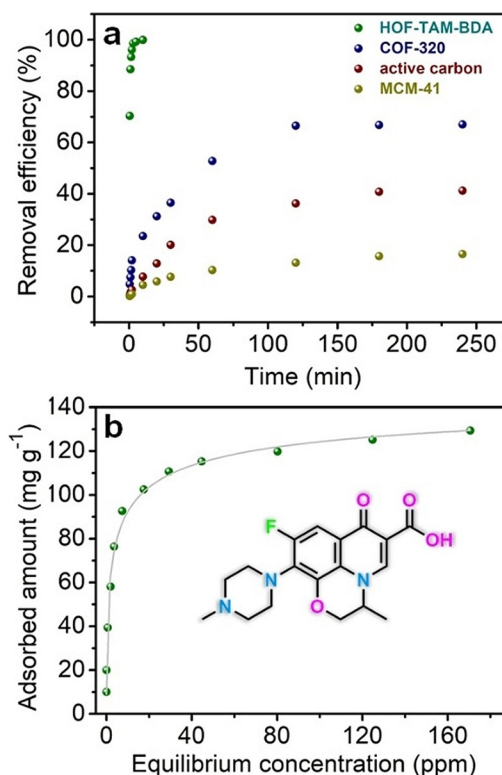


Figure 5. Ofloxacin adsorption performance evaluation. a) Ofloxacin sorption kinetics of various porous materials with initial ofloxacin concentration of 20 ppm at a V_m^{-1} ratio of 1 mL mg⁻¹. b) Ofloxacin adsorption isotherm for HOF-TAM-BDA. Inset: the chemical structure of ofloxacin.

($0.23 \text{ mg g}^{-1} \text{ min}^{-1}$), and MCM-41 ($0.08 \text{ mg g}^{-1} \text{ min}^{-1}$). The equilibrium uptake of HOF-TAM-BDA, as a function of residual ofloxacin amounts, was observed to fit the Langmuir model, and yielded a correlation coefficient higher than 0.99. The maximum adsorption capacity (q_{max}) was determined as 151.5 mg g^{-1} (Figure 5b; Supporting Information, Figure S32). Remarkably, the adsorbed ofloxacin was readily removed from HOF-TAM-BDA by rinsing the reacted material with acetone and exhibited a negligible loss in performance for at least 10 consecutive cycles (Supporting Information, Figure S33).

To elucidate the superior sorption affinity of HOF-TAM-BDA toward ofloxacin, the growth of single crystals was attempted by soaking HOF-TAM-BDA single crystals in an ofloxacin aqueous solution for SCXRD analysis. Unfortunately, the encapsulated guest molecules were highly disordered, which hindered the extraction of the positions. Therefore, DFT calculations were performed to trace the sorbate-sorbent interaction by analyzing the binding site of ofloxacin in HOF-TAM-BDA after energy minimization (Figure 6a, see details in the Supporting Information). The formation of multiple H bonds was noted to facilitate the adsorption of ofloxacin within the framework. Each F atom accepted four

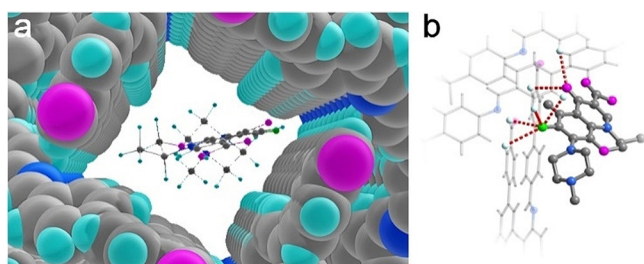


Figure 6. Sorbate-sorbent interaction identification. Optimized geometry of the HOF-TAM-BDA domain after ofloxacin adsorption. To simplify, only one guest molecule was introduced into a $1 \times 2 \times 1$ supercell based on the primitive cell. For clarity, only hydrogen atoms have hydrogen bonding interactions with the guest molecule are shown (C gray, N blue, H light cyan, F green).

hydrogen bonds from HOF-TAM-BDA, three H atoms from phenyl rings with C-H...F distances of 2.179, 2.755, and 3.054 \AA , and one from the aldehyde group, with a C-H...F distance of 2.376 \AA . Additionally, the carbonyl oxygen in ofloxacin was capable of facilitating hydrogen bonding with the sorbent material, and the C-H...O distances were determined to be 2.857 and 2.865 \AA (Figure 6b). Based on these interactions, the resulting structure exhibited a high ofloxacin binding energy of 133 kJ mol^{-1} . Given that these hydrogen bond donors belonged to different strands, their arrangement played an essential role in the formation of the binding network. Therefore, because of the appropriate pore structure and surface chemistry of the resulting HOFs, they exhibited enhanced affinity to pharmaceuticals; this can generally be applied to several other organic micropollutants, and potentially for water purification as well. Fundamentally, the thermodynamic favorability of guest molecule pore-filling was observed to depend more on the strength of the host-guest binding affinity rather than surface area.

To further explore the capabilities of these materials, nanofiltration membrane active layers of HOF-TAM-BDA were synthesized via interfacial polymerization on top of a PAN ultrafiltration membrane support. To evaluate the ofloxacin removal performance of HOF-TAM-BDA/PAN (Supporting Information, Figures S34 and S35), breakthrough experiments were conducted wherein pressure-driven and ofloxacin-spiked water samples were passed through the membrane. High-performance liquid chromatography data revealed that the ofloxacin concentration at the outlet was lower than the detection limit (0.05 ppm), thereby indicating that ofloxacin was completely excluded by the membrane ($>99\%$). Moreover, the membrane exhibited excellent long-term operation stability and maintained the ofloxacin rejection efficiency for at least 24 h, thereby demonstrating the potential versatility of these materials for environmental remediation.

Conclusion

A novel, porous, and organic single-crystal framework was developed using in situ-formed oligomers. The results of this initial study show great promise for the use of covalent and noncovalent bonding to facilitate the direct assembly of new materials. The unique assembly in these HOFs imparted them with excellent hydrolytic stability and binding affinity toward organic micropollutants; these properties were significantly better than those of the COF-320 counterpart. Comparative tests unambiguously revealed differences between these compounds, despite the fact that these materials were constructed using similar starting monomers. The present study is expected to inspire the development of advanced materials, which can eventually lead to the advancement of existing storage, separation, sensing, and catalysis-related technologies.

Acknowledgements

The authors acknowledge the National Science Foundation of China (21776241, 2196116074, 22072132) and the Fundamental Research Funds for the Central Universities (2019XZZX003-04, 17221012001) for financial support of this work. Partial support from the U.S. National Science Foundation (CBET-1706025) and the Robert A. Welch Foundation (B-0027) is also acknowledged.

Conflict of interest

The authors declare no conflict of interest.

Keywords: hydrolytic stability · interfacial polymerization · kinetic conditions · micropollutant removal · porous organic crystals

- [1] a) M. E. Davis, *Nature* **2002**, *417*, 813–821; b) A. Corma, *Chem. Rev.* **1997**, *97*, 2373–2419; c) D. Das, P. Heasman, T. Ben, S. Qiu, *Chem. Rev.* **2017**, *117*, 1515–1563; d) T. A. Makal, J.-R. Li, W. Lu, H.-C. Zhou, *Chem. Soc. Rev.* **2012**, *41*, 7761–7779; e) P. Kuhn, A. Forget, D. Su, A. Thomas, M. Antonietti, *J. Am. Chem. Soc.* **2008**, *130*, 13333–13337; f) W. Li, J. Liu, D. Zhao, *Nat. Rev. Mater.* **2016**, *1*, 16023; g) T. Tozawa, J. T. A. Jones, S. I. Swamy, S. Jiang, D. J. Adams, S. Shakespeare, R. Clowes, D. Bradshaw, T. Hasell, S. Y. Chong, C. Tang, S. Thompson, J. Parker, A. Trewin, J. Bacsá, A. M. Z. Slawin, A. Steiner, A. I. Cooper, *Nat. Mater.* **2009**, *8*, 973–978; h) I. Hisaki, C. Xin, K. Takahashi, T. Nakamura, *Angew. Chem. Int. Ed.* **2019**, *58*, 11160–11170; *Angew. Chem.* **2019**, *131*, 11278–11288; i) M. Mastalerz, I. M. Oppel, *Angew. Chem. Int. Ed.* **2012**, *51*, 5252–5255; *Angew. Chem.* **2012**, *124*, 5345–5348; j) A. Pulido, L. Chen, T. Kaczorowski, D. Holden, M. A. Little, S. Y. Chong, B. J. Slater, D. P. McMahon, B. Bonillo, C. J. Stackhouse, A. Stephenson, C. M. Kane, R. Clowers, T. Hasell, A. I. Cooper, G. M. Day, *Nature* **2017**, *543*, 657–664.
- [2] a) Q. Sun, B. Aguila, Y. Song, S. Ma, *Acc. Chem. Res.* **2020**, *53*, 812–821; b) A. Alsaiee, B. J. Smith, L. Xiao, Y. Ling, D. E. Helbling, W. R. Dichtel, *Nature* **2016**, *529*, 190–194; c) J. Li, X. Dai, L. Zhu, C. Xu, D. Zhang, M. A. Silver, P. Li, L. Chen, Y. Li, D. Zuo, H. Zhang, C. Xiao, J. Chen, J. Diwu, O. K. Farha, T. E. Albrecht-Schmitt, Z. Chai, S. Wang, *Nat. Commun.* **2018**, *9*, 3007; d) R. J. Drout, L. Robison, Z. Chen, T. Islamoglu, O. K. Farha, *Trends Chem.* **2019**, *1*, 304–317.
- [3] a) J. Lü, C. Perez-Krap, M. Suetin, N. H. Alsmail, Y. Yan, S. Yang, W. Lewis, E. Bichoutskaia, C. C. Tang, A. J. Blake, R. Cao, M. Schröder, *J. Am. Chem. Soc.* **2014**, *136*, 12828–12831; b) Y. Lin, X. Jiang, S. T. Kim, S. B. Alahakoon, X. Hou, Z. Zhang, C. M. Thompson, R. A. Smaldone, C. Ke, *J. Am. Chem. Soc.* **2017**, *139*, 7172–7175; c) X. Zhang, L. Li, J.-X. Wang, H.-M. Wen, R. Krishna, H. Wu, W. Zhou, Z.-N. Chen, B. Li, G. Qian, B. Chen, *J. Am. Chem. Soc.* **2020**, *142*, 633–640; d) W. Yang, A. Greenaway, X. Lin, R. Matsuda, A. J. Blake, C. Wilson, W. Lewis, P. Hubberstey, S. Kitagawa, N. R. Champness, M. Schröder, *J. Am. Chem. Soc.* **2010**, *132*, 14457–14469; e) K.-D. Zhang, J. Tian, D. Hanifi, Y. Zhang, A. C.-H. Sue, T.-Y. Zhou, L. Zhang, X. Zhao, Y. Liu, Z.-T. Li, *J. Am. Chem. Soc.* **2013**, *135*, 17913–17918; f) Y.-L. Wu, N. E. Horwitz, K.-S. Chen, D. A. Gomez-Gualdron, N. S. Luu, L. Ma, T. C. Wang, M. C. Hersam, J. T. Hupp, O. K. Farha, R. Q. Snurr, M. R. Wasielewski, *Nat. Chem.* **2017**, *9*, 466–472; g) Q. Yin, P. Zhao, R.-J. Sa, G.-C. Chen, J. Lü, T.-F. Liu, R. Cao, *Angew. Chem. Int. Ed.* **2018**, *57*, 7691–7696; *Angew. Chem.* **2018**, *130*, 7817–7822; h) X.-Z. Luo, X.-J. Jia, J.-H. Deng, J.-L. Zhong, H.-J. Liu, K.-J. Wang, D.-C. Zhong, *J. Am. Chem. Soc.* **2013**, *135*, 11684–11687; i) W. Liang, F. Carraro, M. B. Solomon, S. G. Bell, H. Amenitsch, C. J. Sumby, N. G. White, P. Falcaro, C. J. Doonan, *J. Am. Chem. Soc.* **2019**, *141*, 14298–14305.
- [4] a) K. Shen, L. Zhang, X. Chen, L. Liu, D. Zhang, Y. Han, J. Chen, J. Long, R. Luque, Y. Li, B. Chen, *Science* **2018**, *359*, 206–210; b) C. Gu, N. Hosono, J.-J. Zheng, Y. Sato, S. Kusaka, S. Sakaki, S. Kitagawa, *Science* **2019**, *363*, 387–391; c) P.-Q. Liao, N.-Y. Huang, W.-X. Zhang, J.-P. Zhang, X.-M. Chen, *Science* **2017**, *356*, 1193–1196; d) H. Li, M. Eddaoudi, M. O’Keeffe, O. M. Yaghi, *Nature* **1999**, *402*, 276–279; e) J.-R. Li, J. Sculley, H.-C. Zhou, *Chem. Rev.* **2012**, *112*, 869–932; f) T. Luo, K. Ni, A. Culbert, G. Lan, Z. Li, X. Jiang, M. Kaufmann, W. Lin, *J. Am. Chem. Soc.* **2020**, *142*, 7334–7339; g) A. J. Rieth, A. M. Wright, M. Dincă, *Nat. Rev. Mater.* **2019**, *4*, 708–725; h) X. Han, H. G. W. Godfrey, L. Briggs, A. J. Davies, Y. Cheng, L. L. Daemen, A. M. Sheveleva, F. Tuna, E. J. L. McInnes, J. Sun, C. Drathen, M. W. George, A. J. Ramirez-Cuesta, K. M. Thomas, S. Yang, M. Schröder, *Nat. Mater.* **2018**, *17*, 691–696; i) A. J. Howarth, Y. Liu, P. Li, Z. Li, T. C. Wang, J. T. Hupp, O. K. Farha, *Nat. Rev. Mater.* **2016**, *1*, 15018; j) D. E. Jaramillo, D. A. Reed, H. Z. H. Jiang, J. Oktawiec, M. W. Mara, A. C. Forse, D. J. Lussier, R. A. Murphy, M. Cunningham, V. Colombo, D. K. Shuh, J. A. Reimer, J. R. Long, *Nat. Mater.* **2020**, *19*, 517–521; k) D. Sheberla, J. C. Bachman, J. S. Elias, C.-J. Sun, Y. Shao-Horn, M. Dincă, *Nat. Mater.* **2017**, *16*, 220–224.
- [5] a) Y. Song, Q. Sun, B. Aguila, S. Ma, *Adv. Sci.* **2019**, *6*, 1801410; b) K. Geng, T. He, R. Liu, S. Dalapati, K. T. Tan, Z. Li, S. Tao, Y. Gong, Q. Jiang, D. Jiang, *Chem. Rev.* **2020**, *120*, 8814–8933; c) X. Guan, F. Chen, Q. Fang, S. Qiu, *Chem. Soc. Rev.* **2020**, *49*, 1357–1384; d) X. Han, C. Yuan, B. Hou, L. Liu, H. Li, Y. Liu, Y. Cui, *Chem. Soc. Rev.* **2020**, *49*, 6248–6272; e) S. Kandambeth, K. Dey, R. Banerjee, *J. Am. Chem. Soc.* **2019**, *141*, 1807–1822; f) G. Lin, H. Ding, R. Chen, Z. Peng, B. Wang, *J. Am. Chem. Soc.* **2017**, *139*, 8705–8709; g) M. S. Lohse, T. Bein, *Adv. Funct. Mater.* **2018**, *28*, 1705553; h) D. Beaudoin, T. Maris, J. D. Wuest, *Nat. Chem.* **2013**, *5*, 830–834; i) Y. Jin, Y. Hu, W. Zhang, *Nat. Rev. Chem.* **2017**, *1*, 0056; j) H. M. El-Kaderi, J. R. Hunt, J. L. Mendoza-Cortés, A. P. Côté, R. E. Taylor, M. O’Keeffe, O. M. Yaghi, *Science* **2007**, *316*, 268–272; k) A. P. Côté, A. I. Benin, N. W. Ockwig, M. O’Keeffe, A. J. Matzner, O. M. Yaghi, *Science* **2005**, *310*, 1166–1170; l) A. M. Evans, L. R. Parent, N. C. Flanders, R. P. Bisbey, E. Vitaku, M. S. Kirschner, R. D. Schaller, L. X. Chen, N. C. Gianneschi, W. R. Dichtel, *Science* **2018**, *361*, 52–57; m) E. Jin, M. Asada, Q. Xu, S. Dalapati, M. A. Addicoat, M. A. Brady, H. Xu, T. Nakamura, T. Heine, Q. Chen, D. Jiang, *Science* **2017**, *357*, 673–676.
- [6] a) A. Burgun, C. J. Coghlan, D. M. Huang, W. Chen, S. Horike, S. Kitagawa, J. F. Alvino, G. F. Metha, C. J. Sumby, C. J. Doonan, *Angew. Chem. Int. Ed.* **2017**, *56*, 8412–8416; *Angew. Chem.* **2017**, *129*, 8532–8536; b) B. Chen, S. Xiang, G. Qian, *Acc. Chem. Res.* **2010**, *43*, 1115–1124.
- [7] T. Ma, E. A. Kapustin, S. X. Yin, L. Liang, Z. Zhou, J. Niu, L.-H. Li, Y. Wang, J. Su, J. Li, X. Wang, W. D. Wang, W. Wang, J. Sun, O. M. Yaghi, *Science* **2018**, *361*, 48–52.
- [8] a) J.-H. Dou, M. Q. Arguilla, Y. Luo, J. Li, W. Zhang, L. Sun, J. L. Mancuso, L. Yang, T. Chen, L. R. Parent, G. Skorupskii, N. J. Libretto, C. Sun, M. C. Yang, P. V. Dip, E. J. Brignole, J. T. Miller, J. Kong, C. H. Hendon, J. Sun, M. Dincă, *Nat. Mater.* **2021**, *20*, 222–228; b) D.-G. Ha, M. Rezaee, Y. Han, S. A. Siddiqui, R. W. Day, L. S. Xie, B. J. Modtland, D. A. Muller, J. Kong, P. Kim, M. Dincă, M. A. Baldo, *ACS Cent. Sci.* **2021**, *7*, 104–109.
- [9] Y.-B. Zhang, J. Su, H. Furukawa, Y. Yun, F. Gándara, A. Duong, X. Zou, O. M. Yaghi, *J. Am. Chem. Soc.* **2013**, *135*, 16336–16339.
- [10] E. H. Cordes, W. P. Jencks, *J. Am. Chem. Soc.* **1963**, *85*, 2843–2848.
- [11] a) S. Kandambeth, D. B. Shinde, M. K. Panda, B. Lukose, T. Heine, R. Banerjee, *Angew. Chem. Int. Ed.* **2013**, *52*, 13052–13056; *Angew. Chem.* **2013**, *125*, 13290–13294; b) Y. Peng, L. Li, C. Zhu, B. Chen, M. Zhao, Z. Zhang, Z. Lai, X. Zhang, C. Tan, Y. Han, Y. Zhu, H. Zhang, *J. Am. Chem. Soc.* **2020**, *142*, 13162–13169; c) S. B. Alahakoon, K. Tan, H. Pandey, S. D. Diwakara, G. T. McCandless, D. I. Grinffiel, A. Durand-Silva, T. Thonhauser, R. A. Smaldone, *J. Am. Chem. Soc.* **2020**, *142*, 12987–12994.
- [12] Deposition Numbers 2033511 (for HOF-TAM-BDA), 2033513 (for HOF-TAM-PNA), and 2033512 (for HOF-TAM-BPY) contain the supplementary crystallographic data for this paper. These data are provided free of charge by the joint Cambridge Crystallographic Data Centre and Fachinformationszentrum Karlsruhe Access Structures service www.ccdc.cam.ac.uk/structures.

Manuscript received: March 16, 2021

Accepted manuscript online: April 15, 2021

Version of record online: May 28, 2021